

# Precision Crystal Calorimeters in High Energy Physics: Past, Present and Future

Ren-Yuan Zhu

California Institute of Technology, Pasadena, CA 91125, USA

**Abstract.** Precision crystal calorimeters traditionally play an important role in high energy physics experiments. In the last two decades, it faces a challenge to maintain its precision in a hostile radiation environment. This paper reviews the performance of crystal calorimeters constructed for high energy physics experiments and the progress achieved in understanding crystal's radiation damage as well as in developing high quality scintillating crystals for particle physics. Potential applications of new generation scintillating crystals of high density and high light yield, such as LSO and LYSO, in particle physics experiments is also discussed.

**Keywords:** Calorimeter, Crystal, Radiation Damage

**PACS:** 07.20.Fw; 29.40.Mc; 61.80.Fd

## INTRODUCTION

Total absorption shower counters made of inorganic scintillating crystals have been known for decades for their superb energy resolution and detection efficiency [1]. In high energy and nuclear physics, large arrays of scintillating crystals have been assembled for precision measurements of photons and electrons. The discovery potential of

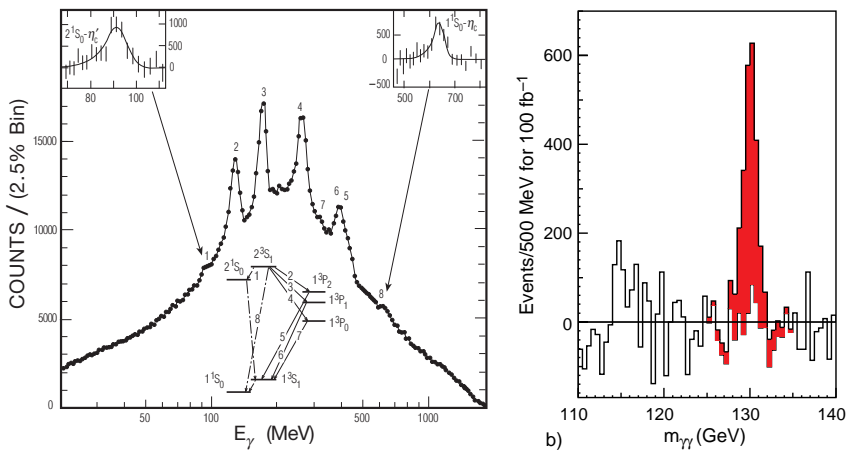


**FIGURE 1.** Left: An inclusive photon spectrum measured at the  $\psi'$  by the NaI(Tl) crystal calorimeter at SLAC [2]. Right: The expected background subtracted Higgs mass peak reconstructed from its two photon decays measured by the CMS PbWO<sub>4</sub> crystal calorimeter [3].

crystal calorimeters was early demonstrated by the Crystal Ball experiment through its study of radiative transitions and decays of the Charmonium family [2]. Figure 1 (Left) shows nearly all the principal radiative transition lines of the Charmonium system simultaneously measured by the NaI(Tl) crystal calorimeter. The designed goal of the CMS lead tungstate ( $\text{PbWO}_4$ ) crystal calorimeter [3] is to maximize its discovery potential in searching for narrow resonances in photon and electron final states at LHC. Figure 1 (Right) shows the expected background subtracted Higgs peak reconstructed with its two decay photons by the CMS  $\text{PbWO}_4$  calorimeter. The potential of the Higgs discovery via this decay channel is directly related to the energy resolution of the calorimeter.

Crystal calorimeters have been constructed, and their use has been a key factor in the successful physics programs of many experiments. With proper calibration and monitoring, crystal calorimeters usually achieve their designed resolution *in situ* [4]. Figure 2 (Left) shows energy resolution as a function of the electron energy obtained with the L3 BGO calorimeter in the CERN test beam, which is in a good agreement with the Bhabha electron resolutions measured *in situ* at LEP by using the RFQ calibration [5], as shown in Figure 2 (Right).

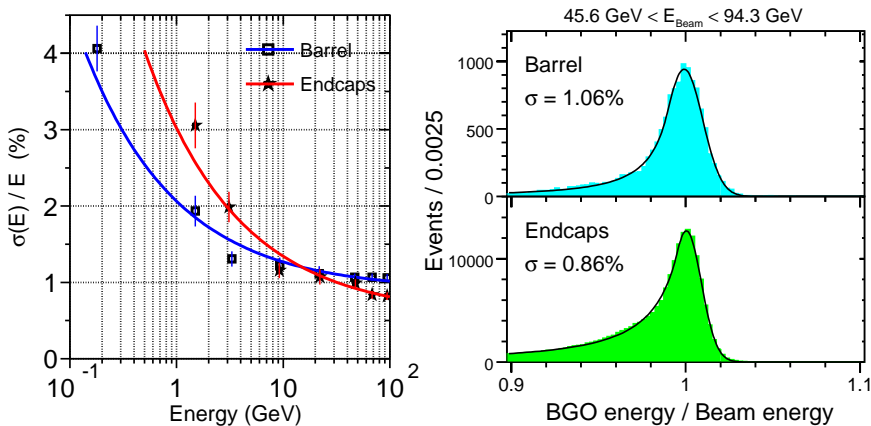


**FIGURE 2.** Left: The energy resolution of the L3 BGO calorimeter as a function of electron energy measured in the CERN test beam. Right: The energy resolution of Bhabha electrons observed by the L3 BGO calorimeter *in situ* at LEP by using the RFQ calibration.

Table 1 summarizes parameters of past and present crystal calorimeters in high energy physics. One notes that each of these calorimeters requires several cubic meters of high quality crystals. The most ambitious crystal calorimeter in Table 1 is presumably the CMS calorimeter which uses  $11 \text{ m}^3$   $\text{PbWO}_4$  crystals. Its designed energy resolution [3] is

$$\sigma_E/E = 2.5\%/\sqrt{E} \oplus 0.55\% \oplus 0.2\%/E \quad (1)$$

for the barrel, and

$$\sigma_E/E = 5.7\%/\sqrt{E} \oplus 0.55\% \oplus 0.25\%/E \quad (2)$$

for the endcaps.

Figure 3 (Left) shows the CMS designed energy resolution as a function of energy. It can be decomposed to three contributions from photoelectron statistics (stochastic),

**TABLE 1.** Crystal Calorimeter in High Energy Physics: Past and Present

Experiment	C. Ball	L3	CLEO II	KTeV	BaBar	BELLE	CMS
Accelerator	SPEAR	LEP	CESR	Tevatron	PEP II	KEK	LHC
Date	75–85	80–00	80–00	90–10	94–10	94–10	95–20
Crystal Type	NaI(Tl)	BGO	CsI(Tl)	CsI	CsI(Tl)	CsI(Tl)	PbWO <sub>4</sub>
B-Field (Tesla)	-	0.5	1.5	-	1.5	1.0	4.0
Inner Radius (m)	0.254	0.55	1.0	-	1.0	1.25	1.29
Number of Crystals	672	11,400	7,800	3,300	6,580	8,800	76,000
Crystal Depth (X <sub>0</sub> )	16	22	16	27	16 to 17.5	16.2	25
Crystal Volume (m <sup>3</sup> )	1	1.5	7	2	5.9	9.5	11
L. Yield (p.e./MeV)	350	1,400	5,000	40	5,000	5,000	2
Photosensor	PMT	Si PD	Si PD	PMT	Si PD	Si PD	APD <sup>†</sup>
Photosensor Gain	Large	1	1	4,000	1	1	50
Noise/Chan. (MeV)	0.05	0.8	0.5	Small	0.15	0.2	30
Dynamic Range	10 <sup>4</sup>	10 <sup>5</sup>	10 <sup>4</sup>	10 <sup>4</sup>	10 <sup>4</sup>	10 <sup>4</sup>	10 <sup>5</sup>

<sup>†</sup> Avalanche photodiode.

intrinsic shower leakage (stochastic and constant) and readout noise (noise). Figure 3 (Right) shows the energy resolution as a function of electron energy measured in the CERN test beam for two groups of  $3 \times 3$  crystals, independent of their impact position on the crystal front face [6]. The measured resolution in the low and middle energy region agrees with the designed resolution. It also shows a smaller constant term because of the perfect calibration in the test beam.

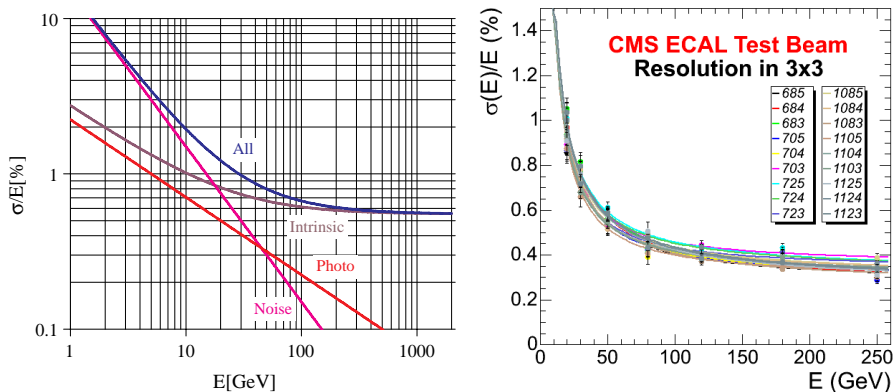


**FIGURE 3.** Left: The designed energy resolution of the CMS PbWO<sub>4</sub> calorimeter is shown as a function of energy and corresponding contributions [3]. Right: The energy resolution of two groups of 9 PbWO<sub>4</sub> crystals is shown as function of electron energy obtained in the CMS ECAL beam test [6].

Over the last two decades, however, crystal calorimeters faced a new challenge: the radiation damage caused by the increased center of mass energy and luminosity. To preserve crystal precision in a severe radiation environment crystal quality control is a crucial issue. The rest of this paper is devoted to a review of optical and scintillation properties of heavy crystal scintillators commonly used for the particle physics. The progresses achieved in understanding crystal's radiation damage and in developing high quality crystals is also be discussed.

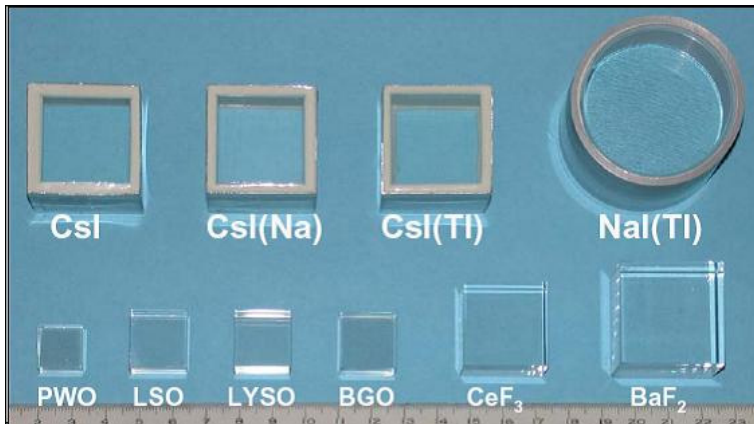
## COMMONLY USED CRYSTAL SCINTILLATORS

Table 2 lists the basic properties of commonly used heavy crystal scintillators: NaI(Tl), CsI(Tl), undoped CsI, BaF<sub>2</sub>, CeF<sub>3</sub>, bismuth germanate (Bi<sub>4</sub>Ge<sub>3</sub>O<sub>12</sub> or BGO), lead tungstate (PbWO<sub>4</sub> or PWO), Ce-doped lutetium oxyorthosilicate (Lu<sub>2</sub>(SiO<sub>4</sub>)O or LSO(Ce)) [7]. Mass production capabilities exist for all these crystals. All, except LSO(Ce) have been used in high energy physics experiments. LSO(Ce) is widely used in the medical industry.

**TABLE 2.** Properties of Heavy Crystal Scintillators with Mass Production Capability

Crystal	NaI(Tl)	CsI(Tl)	CsI	BaF <sub>2</sub>	BGO	PbWO <sub>4</sub>	LSO(Ce)
Density (g/cm <sup>3</sup> )	3.67	4.51	4.51	4.89	7.13	8.3	7.40
Melting Point (°C)	651	621	621	1280	1050	1123	2050
Radiation Length (cm)	2.59	1.86	1.86	2.03	1.12	0.89	1.14
Molière Radius (cm)	4.13	3.57	3.57	3.10	2.23	2.00	2.07
Interaction Length (cm)	42.9	39.3	39.3	30.7	22.8	20.7	20.9
Refractive Index <sup>a</sup>	1.85	1.79	1.95	1.50	2.15	2.20	1.82
Hygroscopicity	Yes	Slight	Slight	No	No	No	No
Luminescence <sup>b</sup> (nm)	410	560	420	300	480	425	420
(at Peak)			310	220		420	
Decay Time <sup>b</sup> (ns)	230	1250	30	630	300	30	40
			6	0.9		10	
Light Yield <sup>b,c</sup>	100	165	3.6	36	21	0.29	83
			1.1	3.4		0.083	
d(LY)/dT <sup>b,d</sup> (%/°C)	-0.2	0.3	-1.3	-1.3	-0.9	-2.7	-0.2
				~0			

- a At the wavelength of the emission maximum.  
 b Top line: slow component, bottom line: fast component.  
 c Relative and PMT quantum efficiency taken out.  
 d At room temperature.



**FIGURE 4.** A photo shows ten crystal scintillators with dimension of 1.5 X 0.

The optical and scintillation properties were measured and compared for various crystal scintillators. Figure 4 is a photo showing ten crystal samples used in this comparative

study. All samples are wrapped with white Tyvek paper as reflectors. NaI and CsI based samples are sealed in quartz window of 3 mm thick to avoid surface degradation caused by their hygroscopicity. To minimize sample size dependence all samples have a cube shape,  $1.5 \times 1.5 \times 1.5 X_0^3$ , except the NaI(Tl) sample which is a cylinder with a length of  $1.5 X_0$  and an area of two ends equal to  $1.5 \times 1.5 X_0^2$  to match the 2 inch diameter of the PMT cathode.

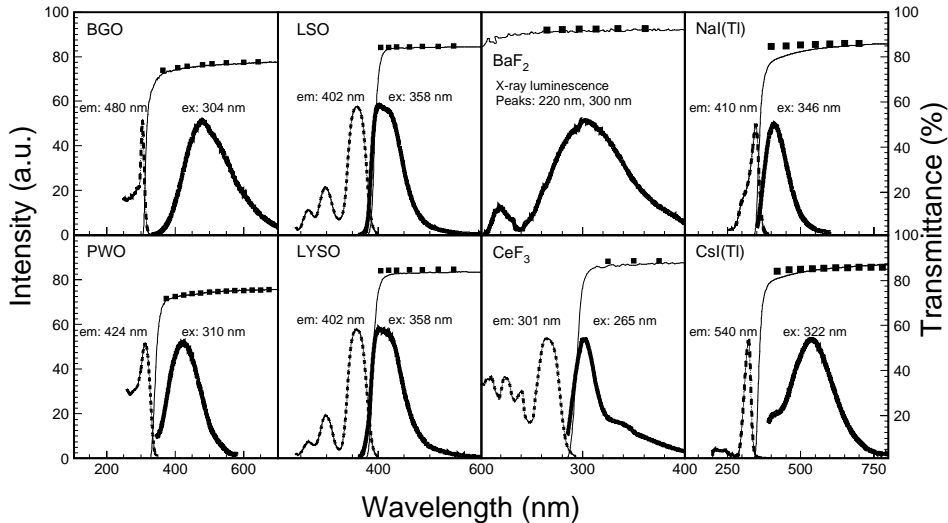


**FIGURE 5.** The excitation (dashed lines) and emission (thick solid lines) spectra (left scale) and the transmittance (thin solid lines) spectra (right scale) are shown as a function of wavelength for eight crystal scintillators.

Figure 5 shows a comparison of the transmittance (thin solid lines), emission (thick solid lines) and excitation (dashed lines) spectra as a function of wavelength for eight samples. The solid black square dots in these plots show the theoretical limit of the transmittance, which was calculated by using corresponding refractive index as a function of wavelength, taking into account multiple bounces between the two parallel end surfaces and assuming no internal absorption [8]. The measured transmittance approaches the theoretical limits, indicating negligible internal absorption. It is interesting to note that while the BGO, BaF<sub>2</sub>, NaI(Tl), PbWO<sub>4</sub> and CsI(Tl) crystals have their emission spectra well within the transparent region, the UV absorption edge in the transmittance spectra of the LSO, LYSO and CeF<sub>3</sub> crystals cuts into the emission spectra and thus affects crystal's light output. This effect is more seriously observed for long LSO and LYSO samples [9].

Figure 6 shows light output in photoelectrons per MeV energy deposition as a function of integration time, measured by using a Photonis XP2254b PMT with multi-alkali photo cathode, for five fast crystal scintillators (Left): LSO, LYSO, CeF<sub>3</sub>, undoped CsI and PbWO<sub>4</sub> and five slow (Right) crystal scintillators: NaI(Tl), CsI(Tl), CsI(Na), BaF<sub>2</sub> and BGO. The undoped CsI, PbWO<sub>4</sub> and BaF<sub>2</sub> crystals are observed to have two decay components as shown in Table 2. The LSO and LYSO samples have consistent fast decay time ( $\sim 40$  ns) and high photoelectron yield, which is 6 and 230 times of BGO

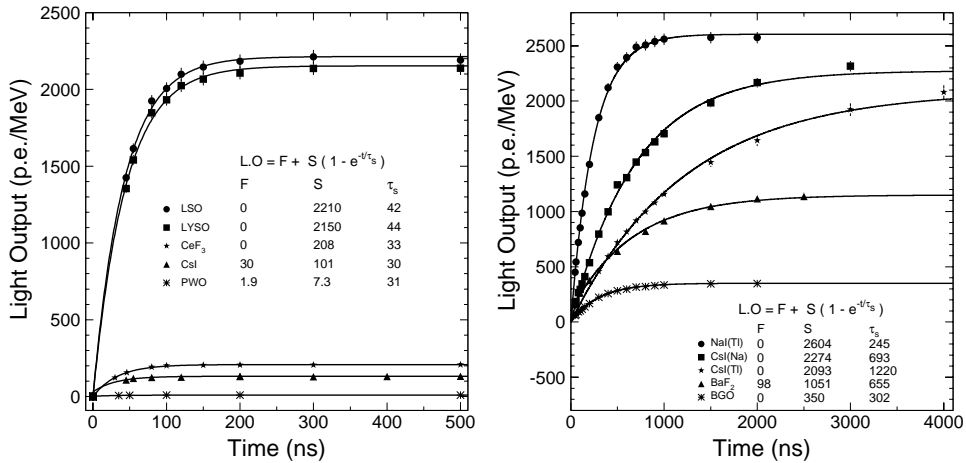


FIGURE 6. Light output measured by using the XP2254b PMT is shown as a function of integration time for five fast (Left) and five slow (Right) crystal scintillators.

and PbWO<sub>4</sub> respectively.

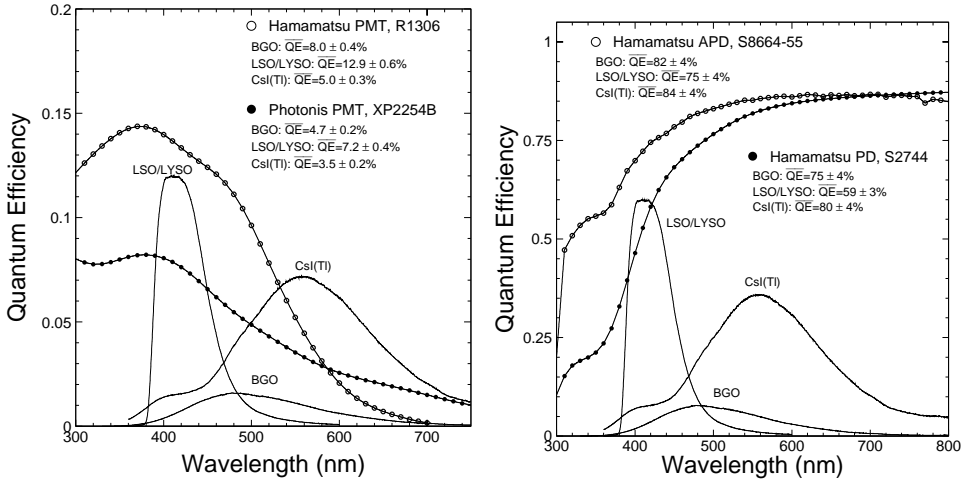


FIGURE 7. Left: The quantum efficiencies of a Hamamatsu 1306 PMT with bi-alkali cathode and a Photonis 2254B (solid dots) PMT with multi-alkali cathode (open circles) are shown as a function of wavelength together with the emission spectra of the LSO/LYSO, BGO and CsI(Tl) samples, where the area under the emission curves is proportional to their corresponding absolute light output. Right: The same for a Hamamatsu S8664 Si APD (open circles) and a Hamamatsu S2744 Si PIN diode (solid dots).

Since the quantum efficiency (QE) of the PMT used for the light output measurement is a function of wavelength, it must be taken out to compare crystal's photon yield. Figure 7 shows typical QE of two PMT with bi-alkali cathode (Hamamatsu R1306) and multi-alkali cathode (Photonis 2254B), a Si APD (Hamamatsu S8664) and a Si PIN PD

(Hamamatsu S2744), as well as the emission spectra of LSO/LYSO, BGO and CsI(Tl) crystals.

**TABLE 3.** Emission Weighted Quantum Efficiencies (%)

Emission	LSO/LYSO	BGO	CsI(Tl)
Hamamatsu R1306 PMT	12.9±0.6	8.0±0.4	5.0±0.3
Hamamatsu R2059 PMT	13.6±0.7	8.0±0.4	5.0±0.3
Photonis XP2254b	7.2±0.4	4.7±0.2	3.5±0.2
Hamamatsu S2744 PD	59±4	75±4	80±4
Hamamatsu S8664 APD	75±4	82±4	84±4

Table 3 summarized numerical result of the emission weighted average QE for several readout devices. Taking into account the PMT response, we conclude that the light output of the LSO and LYSO crystals is a factor of 4 and 200 of that of BGO and PbWO<sub>4</sub> respectively, as shown in Table 2.

Large size LSO and LYSO crystals with consistent optical and scintillation properties have been developed recently for the medical industry. Figure 8 shows four long crystal samples: SIC BGO, CTI LSO, CPI LYSO and Saint-Gobain LYSO of  $2.5 \times 2.5 \times 20$  cm<sup>3</sup> size. Their availability provides a new possibility for the precision crystal calorimeters.



**FIGURE 8.** A photo shows four long crystal samples with dimension of  $2.5 \times 2.5 \times 20$  cm<sup>3</sup>.

Figure 9 shows spectra of 0.51 MeV  $\gamma$ -rays from a <sup>22</sup>Na source observed by these samples with coincidence triggers. The readout devices used are a Hamamatsu R1306 PMT (Left) and 2 Hamamatsu S8664-55 APDs (Right). The FWHM resolution for the 0.51 MeV  $\gamma$ -ray with the PMT readout is about 12% to 13% for the long LSO and LYSO samples, which can be compared to 15% for the BGO sample. With APD readout, the  $\gamma$ -ray peaks are well visible for the long LSO and LYSO samples, but is much less distinguished for the BGO sample. The energy equivalent readout noise in our laboratory set up of APD readout is below 40 keV for the LSO and LYSO samples.

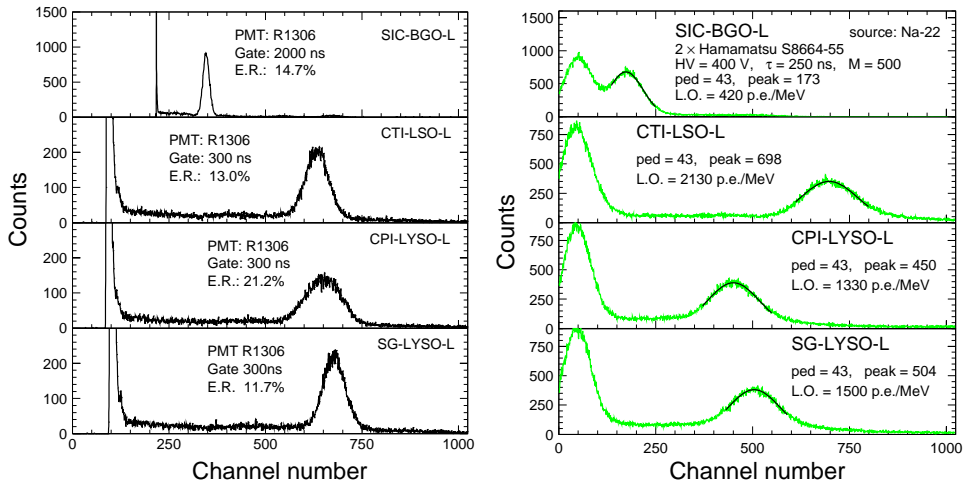


**FIGURE 9.** The spectra of 0.511 MeV  $\gamma$ -rays from a  $^{22}\text{Na}$  source measured with a coincidence trigger using a Hamamatsu R1306 PMT (Left) and two Hamamatsu S8664-55 APDs (Right) for long BGO, LSO and LYSO samples of  $2.5 \times 2.5 \times 20 \text{ cm}^3$  size.

## CRYSTAL RADIATION DAMAGE

All known large size crystal scintillators suffer from radiation damage [10]. There are three possible radiation damage effects in crystal scintillators. First, radiation would induce internal absorption, caused by the color center formation, which would reduce the light attenuation length [8], and thus the light output, and may also cause a degradation of the light response uniformity.

Figure 10 shows the longitudinal transmittance spectra and their degradation under irradiation measured for full size CMS  $\text{PbWO}_4$  (23 cm long, Left) and *BaBar*  $\text{CsI(Tl)}$  (30 cm long, Right) crystal samples respectively. The radiation induced absorption and corresponding color center formation are clearly observed in these samples. Second, radiation would induce phosphorescence (afterglow), which would cause an increase of the readout noise. Last, radiation may also reduce scintillation light yield. If so, both the light output and the light response uniformity would be degraded since the radiation dose profile *in situ* is usually not uniform.

Radiation induced absorption may also recover under application temperature through a process called color center annihilation. If so, the damage would be dose rate dependent [10]. Figures 11 (Left) shows light output normalized to that before irradiation (solid dots with error bars) as a function of time under irradiation for a full size CMS  $\text{PbWO}_4$  sample. Measurements were made step by step for different dose rates: 15, 100, 500 and 1,000 rad/h, as shown in these figures. The degradation of the light output shows a clear dose rate dependence.

If no recovery or the recovery speed is very slow, however, the color center annihilation process would be less important, the color center density would not reach an equilibrium under certain dose rate rather continuously increasing until all defect traps are

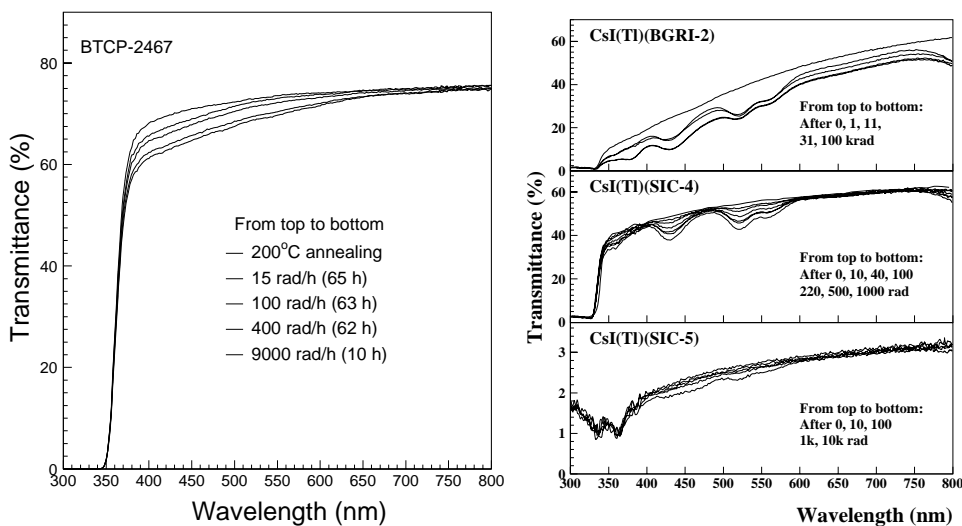


**FIGURE 10.** Longitudinal transmittance of PbWO<sub>4</sub> (Left) and CsI(Tl) (Right) samples, showing radiation induced absorption bands.

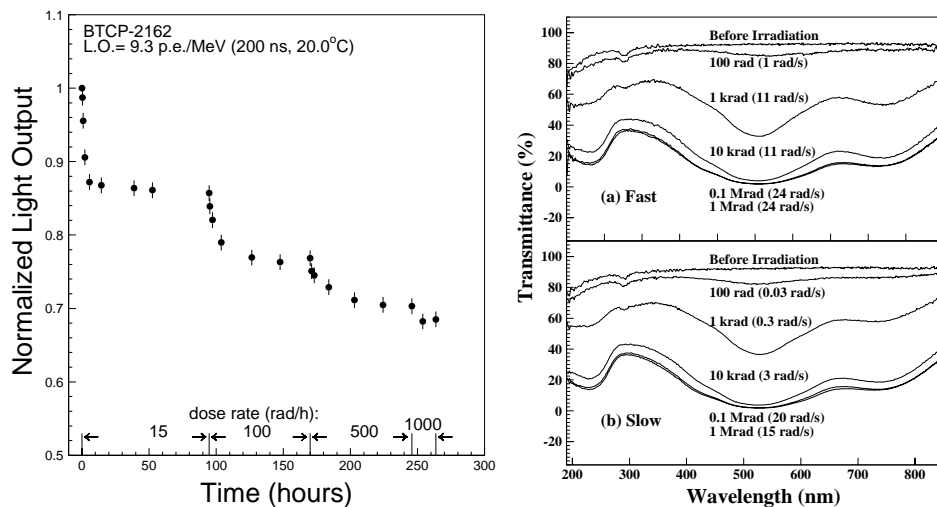


**FIGURE 11.** Left: Normalized light output is plotted as a function of time under irradiations for a CMS PbWO<sub>4</sub> sample, showing dose rate dependent radiation damage. Right: No dose rate dependence was observed for the longitudinal transmittance spectra measured for a GEM full size BaF<sub>2</sub> sample.

filled. This means no dose rate dependence. Figure 11 (Right) shows the transmittance as a function of wavelength for a GEM full size (25 cm) BaF<sub>2</sub> sample before and after 100, 1k, 10k, 100k and 1M rad irradiations (from top to bottom) under a fast (a) and a slow

(b) dose rates. While the fast dose rate is up to a factor of three higher than the slow rate, the damage levels for the same integrated dose are identical. This was expected, since no recovery at room temperature was observed for BaF<sub>2</sub>.

**TABLE 4.** Radiation Damage in Crystal Scintillators

Item	CsI(Tl)	CsI	BaF <sub>2</sub>	BGO	PWO
Color Centers	Yes	Yes	Yes	Yes	Yes
phosphorescence	Yes	Yes	Yes	Yes	Yes
Scintillation Damage	No	No	No	No	No
Recover @RT	Slow	Slow	No	Yes	Yes
Dose Rate Dependence	No	No	No	Yes	Yes
Thermally Annealing	No	No	Yes	Yes	Yes
Optical Bleaching	No	No	Yes	Yes	Yes

Crystal radiation damage may also be cured by either thermal annealing or optical bleaching [11]. Table 4 summarizes radiation damage observed in various crystal scintillators which were used in the high energy and nuclear physics experiments.

For LYSO(Ce) crystals our initial investigation on  $2.5 \times 2.5 \times 20$  cm<sup>3</sup> bar samples indicates that they suffer less radiation damage than other crystals, such as BGO, CsI(Tl) and PbWO<sub>4</sub> [9]. Figure 12 (Left) shows an expanded view of the longitudinal transmittance spectra measured for a long LYSO samples before and after each step of  $\gamma$ -ray irradiations at 2, 100 and 9,000 rad/h. An immediate increase of the longitudinal transmittance after the first irradiation under 2 rad/h was observed, which was followed by small degradation under higher dose rate. Because of LYSO's high light yield its natural phosphorescence and radiation induced phosphorescence have small effect in readout noise. Fig. 12 (Right) shows the  $\gamma$ -ray induced PMT anode current for two long LYSO

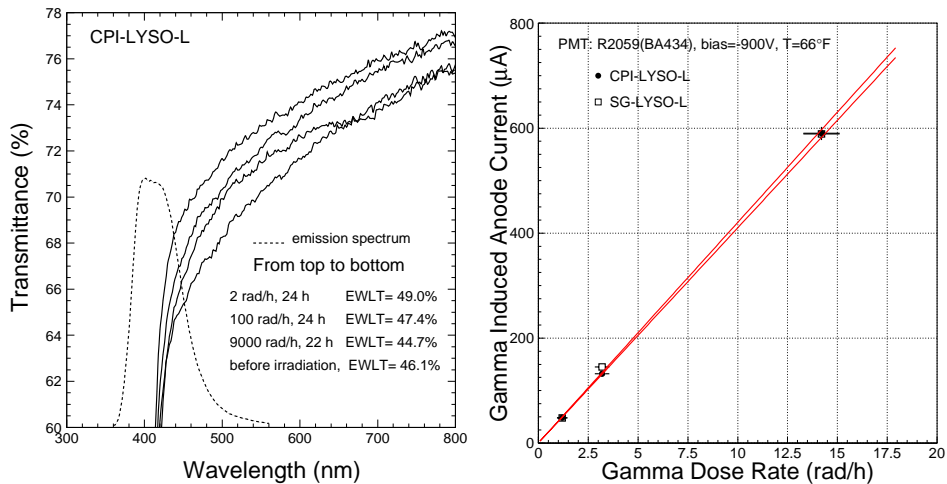


**FIGURE 12.** Left: The longitudinal transmittance spectra before and after 2, 100 and 9,000 rad/h irradiations are shown as a function of wavelength for the Saint-Gobain long LYSO sample. Right: The  $\gamma$ -ray induced anode current is shown as a function of the dose rate for the CPI and Saint-Gobain long LYSO samples.

samples and a linear fit. The radiation induced phosphorescence related readout noise with 100 ns integration time is estimated to be about 0.2 MeV and 1 MeV equivalent respectively in a radiation environment of 15rad/h and 500 rad/h for LYSO samples of  $2.5 \times 2.5 \times 20 \text{ cm}^3$  size.

## CRYSTAL DEVELOPMENT AND QUALITY IMPROVEMENT

Commercially available mass produced crystals usually do not meet the quality required for precision crystal calorimeters. A research and development program is usually needed to systematically study the correlations between crystal's radiation hardness and its impurities and point defects. By removing harmful impurities from the raw materials and developing an approach to effectively reduce the density of defects in the crystal during the growth and processing, the quality of mass produced crystals may be improved. This approach has been successfully carried out for BGO [12],  $\text{BaF}_2$  [13],  $\text{CsI(Tl)}$  [10] and  $\text{PbWO}_4$  [10, 14]. Two examples are given below in this section.

### CsI(Tl) Development

Figure 13 (Left) shows the light output as a function of accumulated dose for full size ( $\sim 30 \text{ cm}$ )  $\text{CsI(Tl)}$  samples produced at the Shanghai Institute of Ceramics (SIC), and compared to the *BaBar* radiation hardness specification (solid line) [10]. While the late

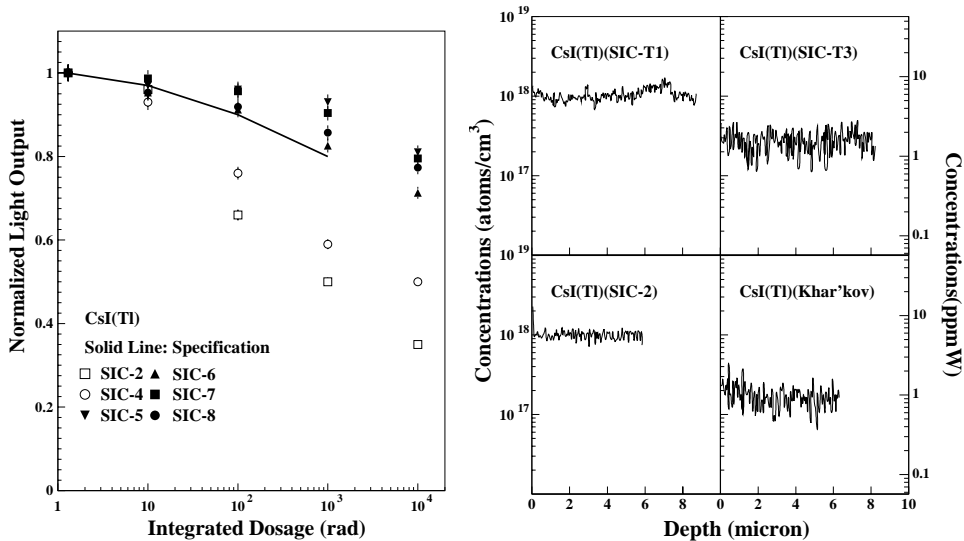


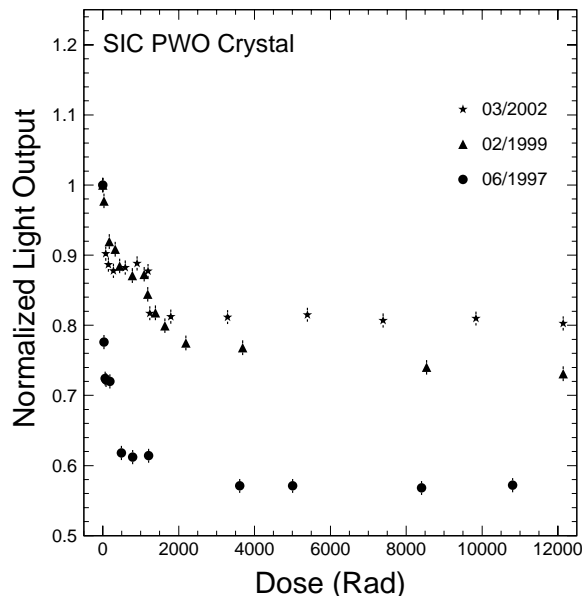
**FIGURE 13.** Left: The progress of  $\text{CsI(Tl)}$  radiation hardness is shown for full size ( $\sim 30 \text{ cm}$ )  $\text{CsI(Tl)}$  samples from SIC together with the rad-hard specification of the *BaBar* experiment. Right: The depth profile of oxygen contamination is shown for two rad-soft  $\text{CsI(Tl)}$  samples (SIC-T1 and SIC-2) and two rad-hard samples (SIC-T3 and Khar'kov).

samples SIC-5, 6, 7 and 8 satisfy the *BaBar* specification, early samples SIC-2 and 4 did not. This improved radiation hardness of CsI(Tl) crystals was also observed by *BaBar* and BELLE experiments [15].

The improvement of CsI(Tl) quality was achieved following an understanding that the radiation damage in halide crystals is caused by the oxygen or hydroxyl contamination. The identification of oxygen contamination was achieved by the Secondary Ionization Mass Spectroscopy (SIMS) analysis carried out at Charles Evans & Associates. A Cs ion beam of 6 keV and 50 nA was used to bombard the CsI(Tl) sample. All samples were freshly cleaved prior before being loaded into the UHV chamber. An area of  $0.15 \times 0.15 \text{ mm}^2$  on the cleaved surface was analyzed. To further avoid surface contamination, the starting point of the analysis is at about  $10 \mu\text{m}$  deep inside the fresh cleaved surface. Figure 13 (Right) shows the depth profile of oxygen contamination for two radiation soft samples (SIC-T1 and SIC-2) and two radiation hard samples (SIC-T3 and Khar'kov). Crystals with poor radiation resistance have oxygen contamination of  $10^{18} \text{ atoms/cm}^3$  or 5.7 ppmW, which is 5 times higher than the background count ( $2 \times 10^{17} \text{ atoms/cm}^3$ , or 1.4 ppmW). The practical solution at SIC is to use a scavenger to remove oxygen. This leads to the development shown in Figure 13 (Left).

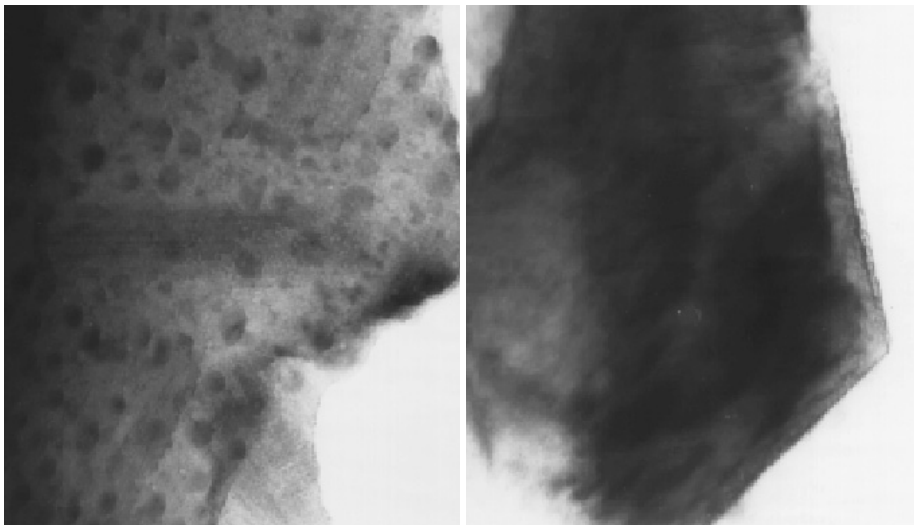
## PbWO<sub>4</sub> Development

Figure 14 shows the light output as a function of time under various dose rates for CMS full size (23 cm) PbWO<sub>4</sub> samples produced at SIC [10]. Samples produced late



**FIGURE 14.** The progress of PbWO<sub>4</sub> radiation hardness is shown for full size (23 cm) CMS PbWO<sub>4</sub> samples from SIC.

2002 is much more radiation hard than the early samples. This improved radiation hardness of  $\text{PbWO}_4$  crystals was also confirmed by an evaluation of mass produced  $\text{PbWO}_4$  crystals [16].



**FIGURE 15.** TEM pictures of a  $\text{PbWO}_4$  crystal of poor (Left) radiation hardness, showing clearly the black spots of  $\phi 5\text{--}10$  nm related to oxygen vacancies, as compared to that of a good one (Right).

The improvement of  $\text{PbWO}_4$  quality was achieved following an understanding that the radiation damage in oxide crystals is caused by the oxygen or lattice structure vacancies. By using Transmission Electron Microscopy (TEM) coupled to Energy Dispersion Spectrometry (EDS), a localized stoichiometry analysis was used to identify oxygen vacancies. A TOPCON-002B Scope was first used at 200 kV and  $10\ \mu\text{A}$ . Samples were made to powders of an average grain size of a few  $\mu\text{m}$ , and then placed on a sustaining membrane. With a spatial resolution of  $2\ \text{\AA}$ , the lattice structure of  $\text{PbWO}_4$  crystals was clearly visible. Figure 15 (Left) shows a TEM picture taken for a sample with poor radiation hardness. Black spots of a diameter of  $5\text{--}10$  nm were clearly seen in the picture. On the other hand, samples with good radiation hardness show stable TEM picture with no black spots, as shown in Figure 15 (Right).

By employing a TEM with EDS system, a localized stoichiometry analysis was carried out at SIC [17]. The system is a JEOL JEM-2010 scope and a Link ISIS EDS. The spatial resolution of this system allows a localized stoichiometry analysis in a region of a diameter of  $0.5\ \text{nm}$ . An as grown sample was first analyzed, and black spots were observed. Points inside and surrounding the black spots were analyzed as well as points far away from the black spots. The uncertainty of the analysis is typically 15%. The resultant atomic fractions (%) at these areas are listed in Table 5. A clear deviation from the atomic stoichiometry of  $\text{O}:\text{W}:\text{Pb} = 66:17:17$  was observed in the center of these black spots, pointing to a severe deficit of the oxygen component. In the peripheral area, the oxygen deficit was less, but still significant. There was no oxygen deficit observed in the area far away from the black spots. As a comparison, the same sample after oxygen

compensation was re-analyzed. No black spot was found. The result of the analysis is also listed in Table 5. In all randomly selected points no stoichiometry deviation was observed. This analysis thus clearly identified oxygen vacancies in  $\text{PbWO}_4$  samples of poor radiation hardness.

**TABLE 5.** Atomic Fraction (%) of O, W and Pb in  $\text{PbWO}_4$  Samples Measured by TEM/EDS [17]  
As Grown Sample

Element	Black Spot	Peripheral	Matrix <sub>1</sub>	Matrix <sub>2</sub>
O	1.5	15.8	60.8	63.2
W	50.8	44.3	19.6	18.4
Pb	47.7	39.9	19.6	18.4

The Same Sample after Oxygen Compensation

Element	Point <sub>1</sub>	Point <sub>2</sub>	Point <sub>3</sub>	Point <sub>4</sub>
O	59.0	66.4	57.4	66.7
W	21.0	16.5	21.3	16.8
Pb	20.0	17.1	21.3	16.5

Various approaches were tried to compensate oxygen vacancies by annealing  $\text{PbWO}_4$  crystals in an oxygen-rich atmosphere [10] and by doping [14]. Significant improvement of radiation hardness was observed in both cases. The practical solution at SIC is to dope  $\text{PbWO}_4$  crystals with yttrium. This leads to the development shown in Figure 14.

## AN LSO/LYSO CRYSTAL CALORIMETER

As discussed in previous sections LSO(Ce) and LYSO(Ce) crystals are a new type of crystal scintillators with light yield 4 and 200 times of BGO and  $\text{PbWO}_4$  respectively and a decay time about 40 ns. The LYSO crystals are also known to suffer less radiation damage as compared to other commonly used crystal scintillators. Mass production capability of LSO/LYSO crystals has been established for the medical industry. Crystals of size sufficient for building a crystal calorimeter are routinely grown. Assuming the same readout scheme as the CMS  $\text{PbWO}_4$  calorimeter, the expected energy resolution of an LSO/LYSO based crystal calorimeter would be

$$\sigma_E/E = 2\%/\sqrt{E} \oplus 0.5\% \oplus 0.001/E, \quad (3)$$

which represents a fast calorimeter over large dynamic range with very low noise. Such calorimeter would provide excellent physics potential for high energy physics experiment in the International Linear Collider [18] or in a super B factory [19].

## SUMMARY

Precision crystal calorimeters have been an important part of high energy physics detector. Its energy resolution, position resolution and photon identification capability has been a key factor in many physics discoveries. In the last two decades, however, it faces a challenge: the radiation damage in scintillation crystals. Progresses have been made in understanding crystal's radiation damage and developing high quality crystals for high energy physics experiments.

Recent availability of mass production capability of large size LSO and LYSO crystals provides an opportunity to build a crystal calorimeter with unprecedented energy resolution over a large dynamic range down to MeV level. This crystal calorimeter, if built, would greatly enhance the discovery potential for future high energy and nuclear physics experiments.

## ACKNOWLEDGMENTS

Work supported by U.S. Department of Energy Grant No. DE-FG03-92-ER40701.

## REFERENCES

1. G. Gratta *et al.*, *Annu. Rev. Nucl. Part. Sci.* **44** 453 (1994).
2. E. Bloom and C. Peck, *Ann. Rev. Nucl. Part. Sci.* 33 143-197 (1983).
3. *The CMS Electromagnetic Calorimeter Project*, CERN/LHCC 97-33 (1997).
4. R.Y. Zhu, *Nucl. Instr. and Meth.* A537 344 (2005).
5. U. Chaturvedi *et al.*, *Nucl. Instr. and Meth.* A461 376 (2001).
6. A. Zabi, in *Proceedings of the 12th International Conference on Calorimetry in Particle Physics*, Chicago, (2006).
7. C. Melcher, V.S. Patent 4958080 (1990) and 5025151 (1991).
8. D.A. Ma and R.Y. Zhu, *Nucl. Instr. and Meth.* A333 (1993) 422.
9. J.M. Chen *et al.*, *IEEE Trans. Nucl. Sci.* **52** (2005) 3133.
10. R.-Y. Zhu, *Nucl. Instr. and Meth.* **A413** (1998) 297–311.
11. D.A. Ma and R.Y. Zhu, *Nucl. Instr. and Meth.* A332 113 (1993) and D.A. Ma *et al.*, *Nucl. Instr. and Meth.* A356 309 (1995).
12. Z.Y. Wei *et al.*, *Nucl. Instr. and Meth.* A297 163 (1990).
13. R.Y. Zhu, *Nucl. Instr. and Meth.* A340 442 (1994).
14. X.D. Qu *et al.*, *Nucl. Instr. and Meth.* **A480**, 470 (2002),
15. T. Hryn'ova, in *Proceedings of the 10th International Conference on Calorimetry in Particle Physics*, World Scientific, Ed. R.-Y. Zhu, 175 (2002).
16. R.H. Mao *et al.*, *IEEE Trans. Nucl. Sci.* **NS-51** (2004) 1777.
17. Z.W. Yin *et al.*, in *Proceedings of SCINT97 Int'l Conf.*, Ed. Zhiwen Yin *et al.*, CAS Shanghai Branch Press, (1997) 191.
18. R.-Y. Zhu, *An LSO/LYSO Crystal Calorimeter for the ILC*, talk presented in 2005 ILC Workshop, Snowmass. See [http://www.hep.caltech.edu/zhu/talks/ryz\\_050818\\_lc.pdf](http://www.hep.caltech.edu/zhu/talks/ryz_050818_lc.pdf).
19. W. Wisniewski, *Consideration for Calorimetry at a Super B Factory*, in *Proceedings of Tenth International Conference on Calorimetry in Particle Physics*, Ed. R.-Y. Zhu, World Scientific (2002).